Nanoparticle Based CT Contrast Agents

Jalil Charmi, Marziyeh Salehiabar, Mohammadreza Ghaffarlou, Hossein Danafar, Taras Kavetskyy, Soodabeh Davaran, Yavuz Nuri Ertas, Surender K. Sharma, and Hamed Nosrati

Abstract The increasing significance of computed tomography (CT) which is one of the most widely used radiological methods in biomedical imaging, has accelerated the development of nanoparticles as next-generation CT contrast agents. Nanoparticles are predicted to play a significant role in the future of medical diagnostics due to

J. Charmi · M. Salehiabar · Y. N. Ertas (✉) · H. Nosrati (✉)
ERNAM—Nanotechnology Research and Application Center, Erciyes University, Kayseri 38039, Turkey
e-mail: yavuzertas@erciyes.edu.tr

H. Nosrati
e-mail: nosrati.hamed2020@gmail.com

M. Ghaffarlou
Department of Chemistry, Hacettepe University, Beytepe, Ankara 06800, Turkey

H. Danafar · H. Nosrati
Zanjan Pharmaceutical Biotechnology Research Center, Zanjan University of Medical Sciences, Zanjan, Iran

H. Danafar · T. Kavetskyy · S. Davaran · H. Nosrati
Joint Ukraine-Azerbaijan International Research and Education Center of Nanobiotechnology and Functional Nanosystems, Drohobych, Ukraine, Baku, Azerbaijan

T. Kavetskyy
Department of Materials Engineering, The John Paul II Catholic University of Lublin, 20-950 Lublin, Poland

Drohobych Ivan Franko State Pedagogical University, Drohobych 82100, Ukraine

S. Davaran
Drug Applied Research Center, Tabriz University of Medical Sciences, 51656-65811 Tabriz, Iran

Y. N. Ertas
Department of Biomedical Engineering, Erciyes University, Kayseri 38039, Turkey

S. K. Sharma
Department of Physics, Central University of Punjab, Bathinda 151401, India

Department of Physics, Federal University of Maranhao, Sao Luis, MA 65080-805, Brazil

S. K. Sharma et al. (eds.), *Harnessing Materials for X-ray Based Cancer Therapy and Imaging*, Nanomedicine and Nanotoxicology,
https://doi.org/10.1007/978-3-031-04071-9_8

their several benefits over conventional contrast agents, such as longer blood circulation time, regulated biological clearance pathways, and precise molecular targeting capabilities. The basic design concepts of nanoparticle-based CT contrast agents will be described in this chapter in comparison to iodine and other commercial products with in vivo and in vitro experiment.

Keywords CT contrast agent · Nanoparticles · X-ray · Medical imaging

1 Introduction

Discovery of X-ray, a milestone in the history of science, has largely been attributed to images from organs to molecules scale in both treatment and diagnosis [1]. Medical application of X-ray is divided into two main categories: structural and functional imaging. Structural imaging reveals anatomical structures, while functional imaging measuring changes in biological functions including metabolism, blood flow, regional chemical composition and biochemical processes [2]. Skipping the various applications of X-ray in non-medical fields such as material science to determine sample structure and physical properties, this chapter is devoted to introducing the benefits of contrast agents and the magnificent role of nanotechnology in developing agents of interest for imaging scope.

Upon X-ray beam incidence and followed interaction with sample, due to the weak X-ray absorption (low attenuation coefficient) with light atoms such as carbon, hydrogen and nitrogen as organic phosphors elements, fluorescence is generated from singlet excitons. Upon X-ray beam incidence and interaction with sample, electrons either attenuation or secondary X-ray/luminescence optical excitation occurs [3, 4]. X-ray may be scattered or absorbed by cells and as a result, X-ray radiation intensity attenuates until it reaches the scintillator. The difference or contrast between different X-ray absorption ability of tissues make it possible to distinguish them [5, 6], whereas the transmitted X-ray generates the background noise [7].

Absorption of X-ray energy by electrons provides a situation for every element to emit a unique X-ray fluorescence spectrum at a specific angle which can be detected by a detector [8]. This spectrum behaves like a fingerprint for identifying the element.

Despite the limitation of imaging techniques, they can be used to complete image information. Contrast agents can also be applied in vivo molecular imaging such as tracking kinetics of drugs, cancer diagnosis and beta-amyloid plaques [9, 10].

X-ray attenuation is detected by projection and computed tomography imaging techniques. The contrast between tissues is determined by relative attenuation of objects which itself depends on atomic number and tissue density [11]. Thus, soft tissues (e.g., tumors, muscle, and fat) and materials containing hydrocarbon backbone with low density and atomic number produce less contrast in comparison to tissues like bone [12].

Computed tomography provides 3D images through mathematical back projection algorithms by converting sinograms to tomograms [13]. This highly efficient imaging

technique apart from many other applications has been used for diagnosis as high resolution data can be analyzed easily. Exposure period must neither be long nor short but long enough to prevent poor resolution, mainly in soft tissue. To increase the quality of the image, several imaging techniques or contrast agents can be employed. Contrast agent material should have a high atomic number to attenuate X-ray intensity to the desired level and consequently, create the appropriate contrast. Commercial contrast agents for examining soft tissue such as iohexol, iodixanol and barium sulfate contain iodine and barium with atomic numbers of 53 and 56 respectively, which enables them to reduce X-ray density more than the soft tissue does.

Disadvantages of conventional X-ray:

- Soft tissues are not distinguished from each other. Although contrast agents are able to enhance the contrast but it has been shown that it is not sufficient for detection of tumors in early stages and in deep anatomical regions.
- Low sensitivity is observed when X-ray intensity decreases, because noise which is caused by transmitted X-ray, lowers the contrast.

Contrast agents can be used for highlighting a specific part of tissue or functionalized to target the expressed proteins on the surface of specific cells such as tumor cells. Not all contrast agents attenuate X-ray intensity at the same level, but proportional to their mass attenuation coefficient. This is the reason why different doses of X-ray are employed for different contrast agents. Toxicity and circulation time of the contrast agent should be taken into consideration for specific applications.

The significance of CT as one of the principal radiology techniques which is frequently used in biomedical imaging, has experienced a significant growth with the development of various nanoparticles (NPs) as next generation CT contrast agents. Because of their numerous benefits over traditional contrast agents, such as longer blood circulation period, regulated biological clearance pathways, and precise molecular targeting capabilities, NPs are going to play a substantial role in the future of medical diagnostics. This section outlines different NPs, which play a significant role in X-ray techniques and imaging applications as contrast agents. Traditionally, iodine-based components were employed as contrast agents in CT scans, however after development of NPs with high atomic number, K-absorption edge (K-edge), and appropriate coefficient absorption, iodine started to lose its importance in the literature. The iodine-based elements were compared to modern NPs such as gold, silver, bismuth, thorium, tantalum, and lanthanides. These series of NPs have usually better performance in comparison to the iodine or iohexol in terms of toxicity, and coefficient parameters. However, thorium-based NPs had a malignancy effect as a long-term side effect. Following sections will provide in-depth information regarding these benefits and deficiencies.

2 Nanoparticle Based Contrast Agents

2.1 Gold Nanoparticle Based Contrast Agents

Gold, one of the chemical elements with high atomic number (79), has been identified as a metaphysical and healing power source since ancient times, and it attracted attention of many researchers in traditional medicine and many of recent investigators were also fascinated by its different applications in nanomaterial and biomedical sciences [14]. In 2004, Smilowitz and his colleagues utilized the high atomic number of gold in the field of X-ray imaging, which has since acquired significant attraction across the world [15]. Since 2004, it is clearly seen that most of the research on inorganic nanoparticles based X-ray contrasting media have focused on gold nanoparticles or their hybrids. Aside from the fact that gold particles exhibit great attenuation in X-ray, research has also concentrated on the significant control of their physical, chemical, and biological characteristics, making it one of the most appropriate candidates for X-ray CT and multimodal imaging [16]. AuNPs are not only stable and inert, but they also exhibit a variety of intriguing characteristics, including self-assembly in conjugation with organization motifs and templates, size-related electrical and optical properties, and uses as catalyst and biological processes. The following points highlight the uses of AuNPs for medical diagnostics and X-ray CT imaging: (i) radiopacity characteristics that have been shown to be superior to standard CT contrast agents (e.g., iodinated), (ii) a highly adaptable and simple surface chemistry that allows for a broad flexibility in surface functionalization for in vivo stability or coating, as well as conjugation with specific functional molecules for active targeting to specific organs and cancerous cells. (iii) and biocompatible properties.

In 1847, Faraday described the production of red gold solutions by reduction of gold chloride and phosphorus in carbon disulfide. Similarly, synthesis process of gold NPs is based on the reduction of gold salt by a variety of reduction agents and chemical methods. Citrate reduction is one of the methods which are introduced by J. Turkevich. This is the simplest protocol which allows the synthesis of monodisperse and spherical shape, citrate stabilized AuNPs with a size range of 10–20 nm [17–19]. However, size of NPs can be changed from 16 to 147 nm using improved methods and adding amphiphilic items into the synthesis reaction [20–23]. In the previous decade, AuNPs were used as X-ray contrast agents due to their high stability against oxidation, exceptional absorption coefficient (5.16 cm^2g^{-1}) and high Z-number (79) instead of traditional iodine-based alternatives with low absorption coefficient (1.94 cm^2g^{-1}) and lower Z-number (53) where Au exhibits 2.7 times more contrast per unit weight in comparison to iodine at 100 keV. Furthermore, gold imaging at 80–100 keV minimizes interferences from bone and soft tissue absorption and finally lowers the overall radiation dosage and exposure [24].

When AuNPs are used as blood pool contrast agents (BPCA), it is worth noting these three factors: (i) stabilization of AuNPs suspensions in bulk media is required which is related to the synthesis steps, (ii) AuNPs should demonstrate proper in vivo

pharmacokinetics properties and good in vivo stability which need suitable coating, for example PEG-coatings which show poor interactions with plasma proteins [19, 20], (iii) active targeting should be achieved by surface modifications to enable site-specific targeting between AuNPs and receptors of tumor cells. Active targeting usually links the functionalized NPs and receptor-specific target using three distinct biomarkers that are highly expressed in cancer cells site which include epidermal growth-factor receptor, matrix metalloprotease and oncoproteins that are related to the human papillomavirus infection [25]. Figure 1 depicts the surface functionalization of AuNPs as well as their potential for surface coating and nano encapsulation. Table 1 shows different applications of AuNPs in BPCA and CT applications. In

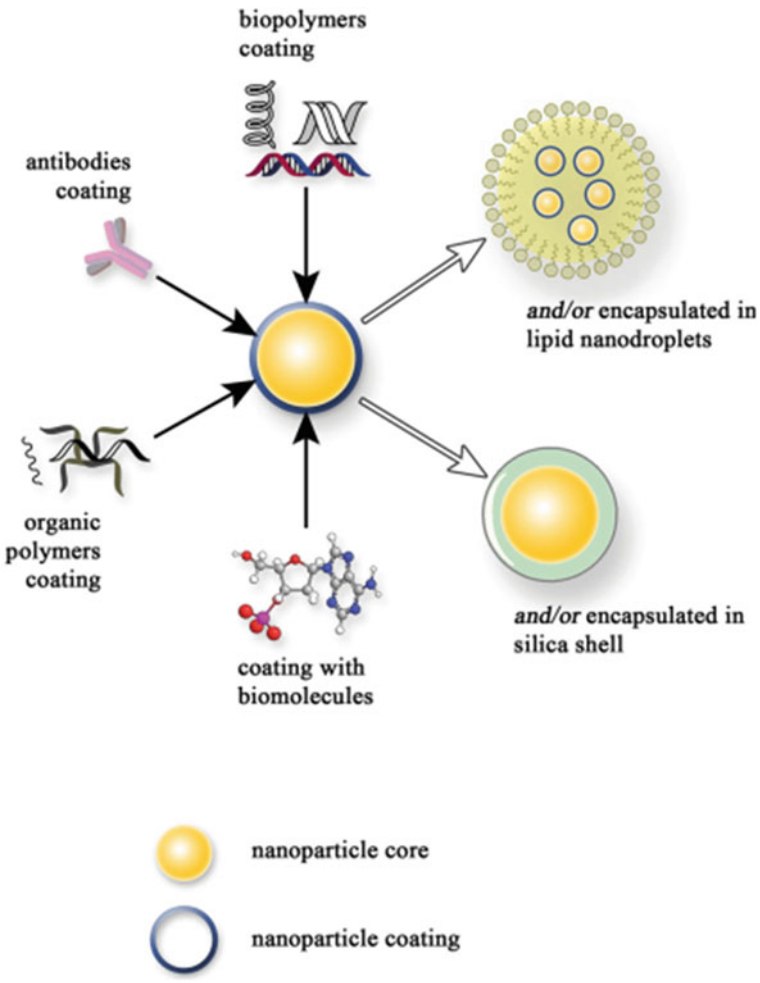

Fig. 1 Schematic illustration of surface functionalization of inorganic NPs with different materials. Reproduced with permission from Ref. [27]. Copyright 2012, with permission from Wiley

Table 1 Main results regarding the use of AuNPs as X-ray contrast agent and imaging

Reducing agent	Coating	Targeting	Application	Main results	References
Citrate	PEG coating	–	BPCA	$t_{1/2}$∼12 h	[19]
Commercial product	Heparin coating	–	Contrast agent	Stable, biocompatible	[28]
THPAL (phosphino animoacid)	Gum Arabic coating	–	Contrast agent	Enhanced contrast in juvenile swine & Good tolerance to administration	[29]
Citrate	2-mercaptosuccinic acid (MSA)	–	Contrast agent	Surface-enhanced Raman spectroscopy (SERS) and CT	[21]
Citrate	PEG-COOH coating	Antibody: CD4	Imaging	Contrast enhancement stronger with large AuNPs	[22]
Growth method	Poly(acrylic acid) (PAA) coating	Antibody: UM-A9	Imaging	CT imaging allows reliable and sensitive detection of lymph nodes	[16]
$NaBH_4$	Dendrimer G5-NH2	Folic-Acid and FITC	Imaging	Efficiency in targeting (and thus imaging) KB cells	[30]

addition, Table 1 shows that citrate reduction is obviously the preferable method for the production of AuNPs core because it is the simplest approach to provide a stable dispersion in aqueous media. Besides, PEGylation of AuNPs can also be beneficiary in BPCA applications and imaging processes, and it can mitigate the effect of reticuloendothelial system (RES) by minimizing the accumulation of AuNPs in liver and spleen. Targeted CT contrast agents using AuNPs have achieved global success ranging from long circulation vascular contrast to targeting tumor cells [19, 20, 22, 26].

To increase contrast effect and better surface modification, gold NPs can be used with gadolinium to provide hybrid NPs. Gadolinium is in the middle of the lanthanide family and it contains seven unpaired electrons, producing a strong signal in magnetic resonance imaging (MRI). Coupling gold with gadolinium illustrates a suitable detectable dual nanosystem both by X-Ray CT and MRI. The core of this hybrid nanosystem is made up of AuNPs and the shell layer is gadolinium where disulfide bonds keep them together. The reduction of gold salt in the presence of dithiolated derivatives of diethylenetriaminepentaacetic acid was followed by the addition of Gd^{3+}. Through disulfide connections, the two thiol groups were critical in the creation of the multilayered ligand shell. Favorably, modest concentrations of

gold (10 mg/mL) and gadolinium (5 mg/mL) could be easily identified and tracked using MRI and X-ray imaging [31]. Presence of cysteine [32], penicillamine [33] and 4-aminothiophenol [34] on Gd added AuNPs demonstrated high r_1 relaxivity [33].

Furthermore, Jon et al. also evaluated the ability of coupled superparamagnetic iron oxide with AuNPs [35, 36]. In 2009, synthesis of PEG coated iron oxide core and gold shell hybrid NPs were also reported. The particle surfaces were coated with PEG to assure biocompatibility and a lengthy circulation duration in the bloodstream even at high concentrations. Amphiphilic poly(DMA-r-mPEGMA-r-MA) prevent aggregation and increasing water solubility [35]. Mulder and colleagues demonstrated another method for developing multifunctional probes for fluorescence imaging, CT, and MRI. They coated a fluorescent and paramagnetic lipid layer containing a Gd conjugation and a special dye Cy5.5 over gold/silica core-shell NPs which exhibited highly sensitive signal enhancements of 24 and 50% for MRI and CT in mice liver, respectively [37].

In another study, Salehi et al. used PEGylated AuNPs with deoxycholic acid (DCA-PEG-GNPs) (Fig. 2c) in comparison to commercially available contrast agent Visipaque. DCA-PEG-GNPs with the size of 17 nm in an oval-like shape as shown in Fig. 2a demonstrated significant stability in a various range of pHs (2.5–11) and

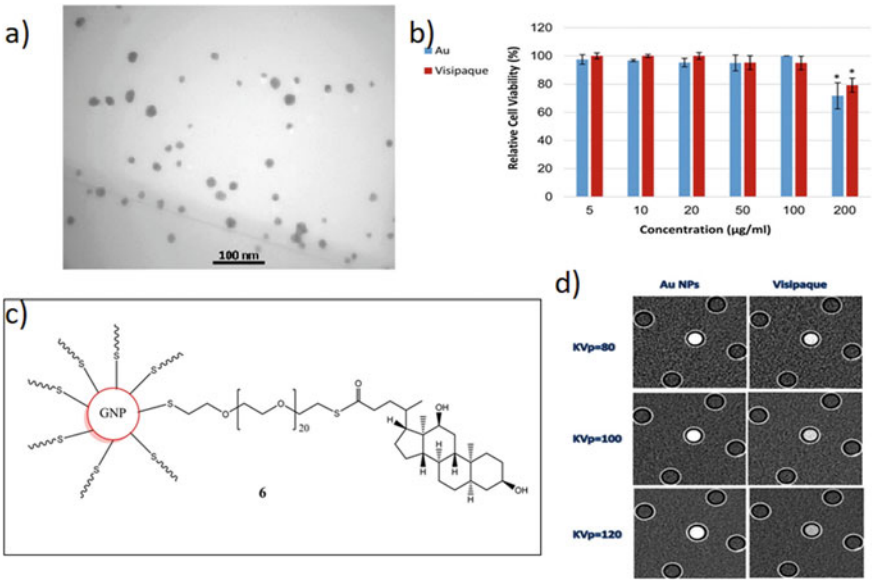

Fig. 2 **a** TEM image of DCA-PEG-GNPs, **b** MTT assay on A549 cells in different concentrations of DCA-PEG-GNPs and Visipaque, **c** Structure of DCA-PEG-GNPs, **d** In vitro X-ray CT images at different kVp values, the vials contained 1.0 mg ml^{-1} AuNPs or iodine. Reproduced with permission from Ref. [38]. Copyright 2020, with permission from Wiley

temperatures (−78–48 °C). Also, AuNPs had similar cell viability with Visipaque in the concentration value of under 100 μg/ml on A549 lung cells. MTT assay also suggested that in the high concentration (200 μg/ml), AuNPs showed low cell viability than Visipaque as shown in Fig. 2b. Notably, CT performance of DCA-PEG-GNPs were higher than Visipaque. This result is also comparable with the iodine. For example, at kVp = 120 keV, the attenuation value of 0.8 mg ml^{-1} for iodine was close to the attenuation value of 0.49 mg ml^{-1} for gold as shown in Fig. 2d [38]. In addition, Wang and his colleagues designed Au nanocage@PEG nanoparticles (AuNC@PEGs) as shown in Fig. 3 in different concentrations (0, 50, 100, 200, 500, and 1000 μg/ml) and compared with iodine and showed that Au nanocages were possible alternative CT contrast agents to iodine [39]. Park et al. synthesized gold@silica NPs, and their cytotoxicity studies displayed that they were not hazardous, and while tiny deformations on the silica shell had no effect on the stability of gold@silica NPs, larger deformations on the silica shell resulted in agglomeration. However, in vivo applications revealed effective contrast enhancement in CT imaging [40]. Real-time in vivo X-ray images showed that gold@silica NPs with folic acid (FA) as a targeting agent can visualize MGC803 gastric cancer after intravenous injection in nude mice as show in Fig. 4 [41, 42].

Interestingly, Guo et al. designed multifunctional core–shell tecto dendrimers (CSTDs) with AuNPs core and β-cyclodextrin modified generation 5 poly(amidoamine) dendrimers for dual-mode CT and MRI of tumors. Au CSTDs with the size of 11.61 nm displayed excellent stability, strong X-ray attenuation and good r_1 relaxivity (9.414 mM^{-1} s^{-1}), and desirable cytocompatibility as well. They also showed that CSTDs act as suitable CT/MRI dual mode imaging probe (Au/Gd) in cancer diagnosis applications as shown in Fig. 5 [43].

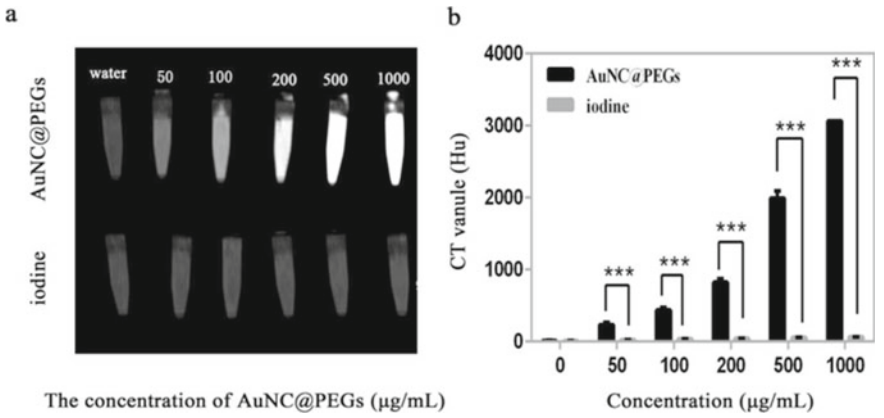

Fig. 3 **a** In vitro CT images of AuNC@PEGs and iodine-based at different concentrations. **b** Hu values for AuNC@PEGs and iodine-based contrast agents, ***P < 0.001. Reproduced from Ref. [39] with the permission of the Creative Commons Attribution 4.0 International License http://creativecommons.org/licenses/by/4.0/). Copyright 2020, Springer

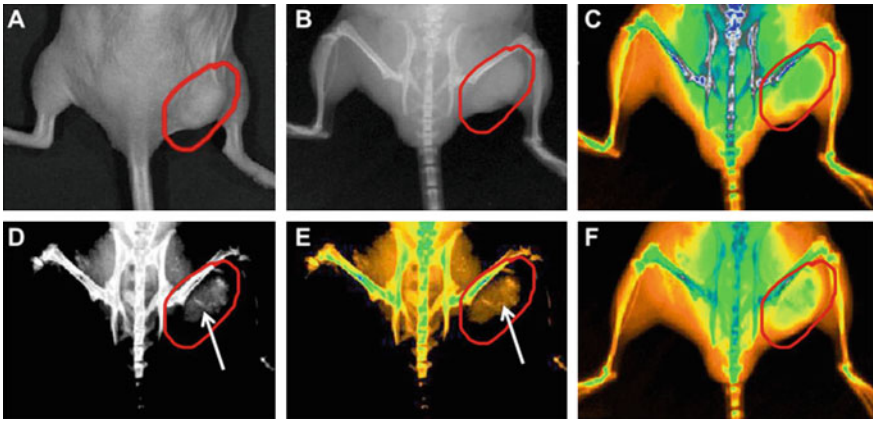

Fig. 4 Real-time in vivo X-ray images. **a** The tumor tissue, **b** X-ray image at 0 h, **c** X-ray image at 0 h (in color), **d** X-ray image at 12 h, **e** X-ray image at 12 h (in color). **f** X-ray image at 24 h (in color). Reproduced with permission from Ref. [41]. Copyright 2011, with permission from Elsevier

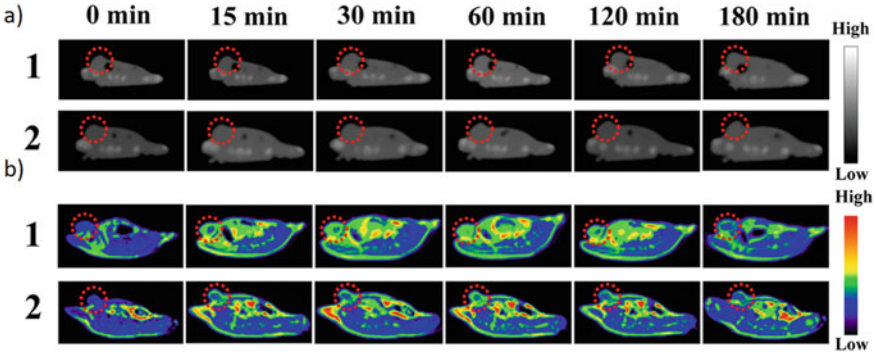

Fig. 5 **a** CT images and **b** T1-weighted MR image of Gd@Au CSTDs in vivo. Reproduced with permission from Ref. [43] Copyright 2021, with permission from ACS

2.2 Silver Nanoparticle Based Contrast Agents

Silver, a metal with atomic number of 47, is recognized as fascinating NPs in different applications such as biomedical sciences, food, textiles, consumer products and industrial purposes, due to their unique physical and chemical properties.

Image processing at two separate energy windows is known as dual-energy imaging (low and high) where images with reduced contrast between background tissues is achieved by weighting variables. Because of good X-ray attenuation properties of Ag as appealing contrast material with k-edge[1] of 25.5 keV and average

[1] The K-absorption edge (K-edge) is the sudden rise in photoelectric absorption of x-ray photons observed at an energy level slightly above the binding energy of the absorbing atom's k-shell

diameter of 2–6 nm by Brust method demonstrate slight cellular toxicity in T6-17 fibroblast cells. AgNPs, stabilized with PEG, can provide similar or better contrast in comparison to the iodine [44].

Silver iodide (AgI) and silver oxide (Ag_2O) were introduced as contrast agents in the earlier twentieth century. However, their usage was immediately halted due to the significant toxicity and reported deaths [45–47]. Yet, silver was maintained in the liver for a long enough period of time to allow CT scanning with a contrast difference of 4–5 times that of the background [48]. Lui et al. showed the X-ray contrasting properties of generation 5 poly(amidoamine) dendrimer which is appropriate for the stabilization of silver nanoparticles for in vivo CT imaging. Size and concentration of AgNPs are two main parameters for the X-ray absorption coefficient. They were not only able to readily control the size of AgNPs from 8.8 to 23.2 nm by changing the molar ratio of dendrimer/Ag salt, but also kept AgNPs stable in the phosphate buffered saline, fetal bovine serum and water at pH range of 5–8 in room temperature conditions. It is quite interesting to note that X-ray attenuation behavior of particles with a diameter of around 16 nm were identical to those of an iodine-based contrast agent and in vivo studies with mice revealed that the AgNPs provided sustained contrast enhancement while having no severe toxicity. In another study, Cormode and his colleagues explored potential of silver telluride (Ag_2Te) NPs in an in vivo setting at a low dose (2 mg Ag per kg) for X-ray imaging. An astonishing contrast agent performance was observed compared to the $AgNO_3$, Na_2TeO_3 and iodine which were frequently used in the previous studies as shown in Fig. 6 [49].

Luo et al. produced heterostructure samples with bismuth and silver NPs conjugated with poly(vinylpyrrolidone) (PVP) to design Bi-Ag@PVP NPs for

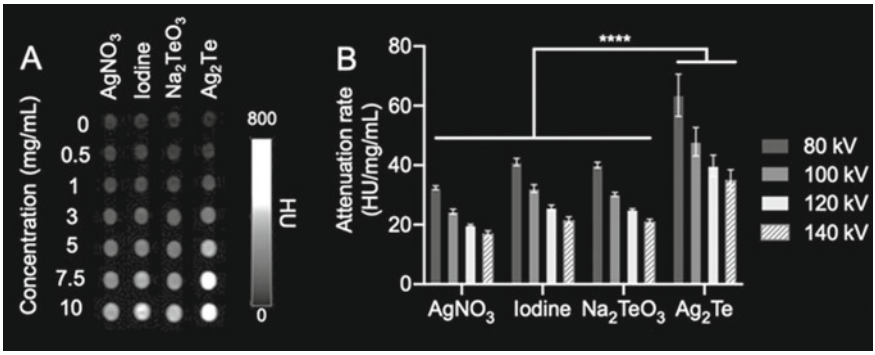

Fig. 6 In vitro imaging with CT. **a** CT phantom images, **b** CT attenuation rate of the different samples at various energies (80,100, 120, and 140 kV). Reproduced with permission from Ref. [49]. Copyright 2020, with permission from RSC

electrons. Each element's K-shell binding energies are unique. As an element's atomic number (Z) grows, so does its corresponding k-shell binding energy, and therefore the photon energy at which the K-edge occurs. The K-edges of the most common elements in human tissue (hydrogen, carbon, oxygen, and nitrogen) are too low to be detected (1 keV). Elements with larger K-edge values, are within the useful portion of the x-ray spectrum, are of greater interest in radiology.

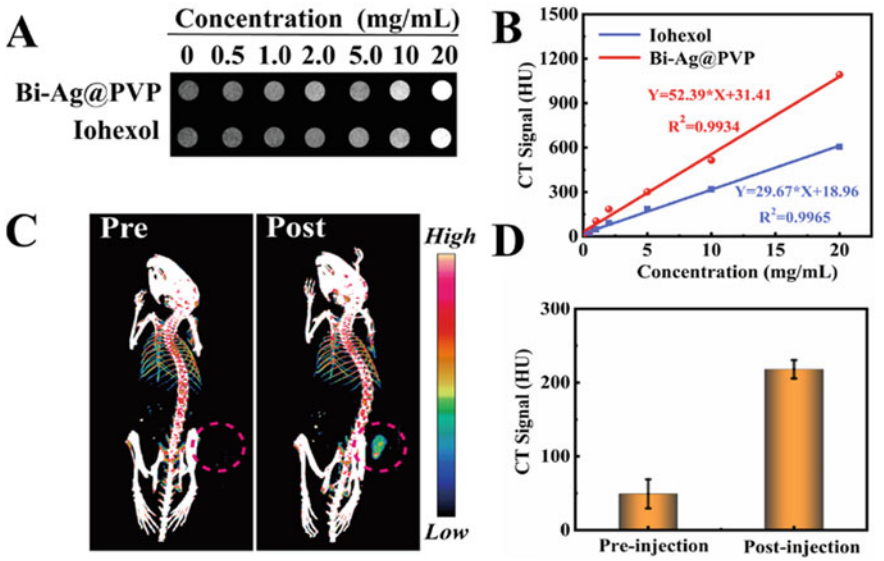

Fig. 7 **a** CT images of Bi-Ag@PVP and iohexol, **b** CT signals-concentration fitting curves, **c** CT imaging capability of Bi-Ag@PVP NPs in tumor site (red), and **d** CT signal intensity before and after injection. Reproduced from Ref. [50] with the permission of the Creative Commons Attribution 4.0 International License http://creativecommons.org/licenses/by/4.0/. Copyright 2021, ACS

quadra applications including CT, photoacoustic imaging, photodynamic therapy and photothermal therapy (PDT/PTT) into one nanotheranostic platform. They also compared Bi-Ag@PVP with the commercial contrast agent, iohexol, in different range concentrations from 0 to 20 mg ml^{-1} as shown in Fig. 7 [50].

2.3 Bi Nanoparticle Based Contrast Agents

Bismuth is a heavy metal with a high atomic number of 83. Bismuth was one of the first X-ray contrast agents used on human gastrointestinal tract before the 1990s [51–53]. The surface of Bi_2S_3 NPs was modified with poly(vinylpyrrolidone) (PVP), a biocompatible polymer, and a rectangular flat plate morphology, size range of 10–50 nm and 4 nm in thickness was obtained. These NPs were highly soluble in water, inert and had a longer blood half-life. Noticeably, the X-ray opacity of Bi_2S_3–PVP NPs was about fivefold higher than the commercial iodine. In vivo experiment revealed the temporal evolution of the blood after injection where NPs accumulated in liver and spleen after 24 h [53].

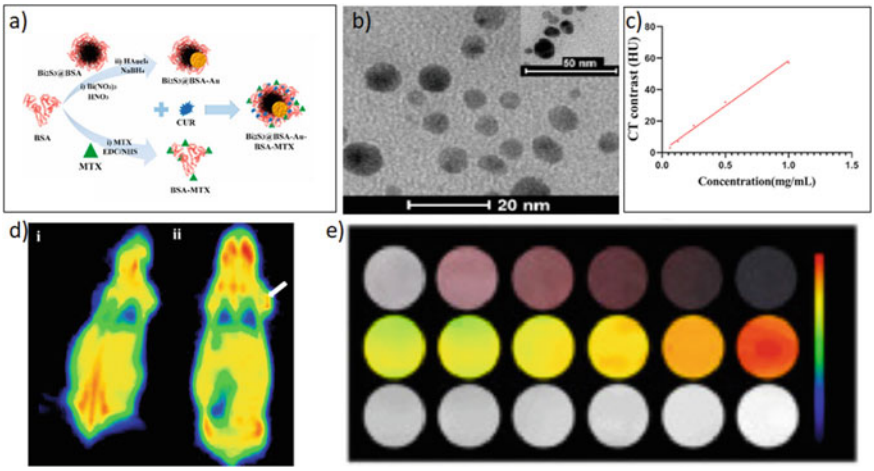

Fig. 8 **a** Schematics of designed nano drug delivery system of Bi_2S_3@BSA-Au-BSA-MTX-CUR, **b** TEM image of Bi_2S_3@BSA-Au-BSA-MTX-CUR, **c** CT contrast value curve of Bi_2S_3@BSA-Au-BSA-MTX-CUR at different concentrations, **d** CT images of mice with a 4T1 tumor recorded at (i) pre and (ii) post intravenous injection of Bi_2S_3@BSA-Au-BSA-MTX-CUR, and **e** First row: Typical photograph of each concentration; Second and Third rows: CT images of each concentration. Reproduced from Ref. [10] with the permission of the Creative Commons Attribution 4.0 International License (http://creativecommons.org/licenses/by/4.0/). Copyright 2022, Elsevier

Radiopaque[2] objects block radiation rather than allow it to pass through. This concept was cleverly employed in a study where Bi_2S_3 NPs with the inner core layer covered with alginate-poly-L-lysine-alginate were used to avoid toxic effects in the X-ray process. Results displayed microcapsules were not only visualized individually in the rabbit and mice, but also kept their contrast properties for two weeks due to low water solubility [54].

Nosrati et al. evaluated the ability of Bi_2S_3-Au semiconductor heterojunction NPs which can improve the contrast of CT images and free radical generation via the Schottky barrier in addition to their intrinsic radiosensitizing ability [10]. As it is declared earlier, under X-ray irradiation, NPs with high-Z number (here bismuth) components produce secondary and Auger electrons via the photoelectric and Compton processes, resulting in the generation of large quantities of reactive oxygen species (ROS) within the cells [10, 55, 56]. Figure 8 shows successful targeting and

[2] **Radiopaque**: Opaque to one or another form of radiation, such as X-rays. Radiopaque Metal, for instance, is radiopaque, so metal objects that a patient may have swallowed are visible on X-rays. Radiopaque dyes are used in radiology to enhance X-ray pictures of internal anatomic structures. The opposite of radiopaque is radiolucent.

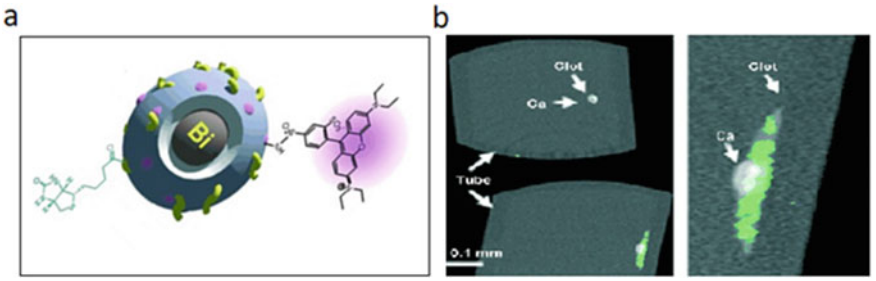

Fig. 9 **a** Structure of Bi-based NanoK, **b** Cross-sectional slices of fibrin clot targeted with NanoK presenting calcium. Reproduced with permission from Ref. [57]. Copyright 2020, with permission from ACS

effective tumor accumulation of drug loaded heterojunction NPs (Bi_2S_3@BSA-Au-BSA-MTX-CUR). It increase the Hounsfield units (HU)[3] in the tumor site from 15 to 81 (white arrow). They also showed that CT contrast intensity directly depended on the concentration of the final sample (Bi_2S_3@BSA-Au-BSA-MTX-CUR) as shown in Fig. 8c and e.

In a study, Pan et al. demonstrated CT contrast effect for detection of clot with thrombus-targeted NanoK with a diameter of 180 and 250 nm (Fig. 9b) [57].

Zhang et al. explored ultrasmall FA and bovine serum albumin-modified Bi–Bi_2S_3 heterostructure NPs (Bi–Bi_2S_3/BSA&FA NPs) as CT contrast agents. Bi–Bi_2S_3/BSA&FA NPs with the size of 10 nm showed not only an appropriate stability due to formation of Bi_2S_3 NPs on the surface of Bi without any agglomeration even after the one month, also displayed photothermal conversion efficiency (35%). As demonstrated in Fig. 10, the X-ray absorption coefficient of Bi–Bi_2S_3/BSA&FA NPs (50.4 HU L g^{-1}) is higher than commercial contrast agent iohexol (24.1 HU L g^{-1}), therefore, Bi–Bi_2S_3/BSA&FA NPs can be a candidate CT contrast agent [58].

Yang et al. explored bismuth functionalized S-nitrosothiol (Bi–SNO NPs) with a size of 36 nm for the combination therapy (X-ray radiotherapy and 808 nm PTT). X-rays can break down the S–N bond and commence a large amount of NO-release which is a cancer killing agent at concentrations above 60 μM [59]. CT value increased from 47.52 HU to 232.21 HU at a NP concentration of 2 mg.mL^{-1} after the injection [59]. Shan et al. designed Bi/Se NPs loaded with Lenvatinib (Len) in a simple reduction reaction for in vivo CT imaging of mice. They showed that Bi/Se-Len NPs can increase CT value from 27 to 638 HU after the injection in mice [60]. Luo and his colleagues also designed hybrid NPs containing bismuth and lanthanide conjugated PVP as BiF_3Ln@PVP as a CT contrasting agent. CT value increased from 48.9 HU to 194.58 HU post-injection, as shown in Fig. 11 [61].

[3] **Hounsfield unit (HU)** is a relative quantitative measurement of radio density that radiologists use to analyze computed tomography (CT) images. During CT reconstruction, the absorption/attenuation coefficient of radiation within a tissue is utilized to generate a grayscale image.

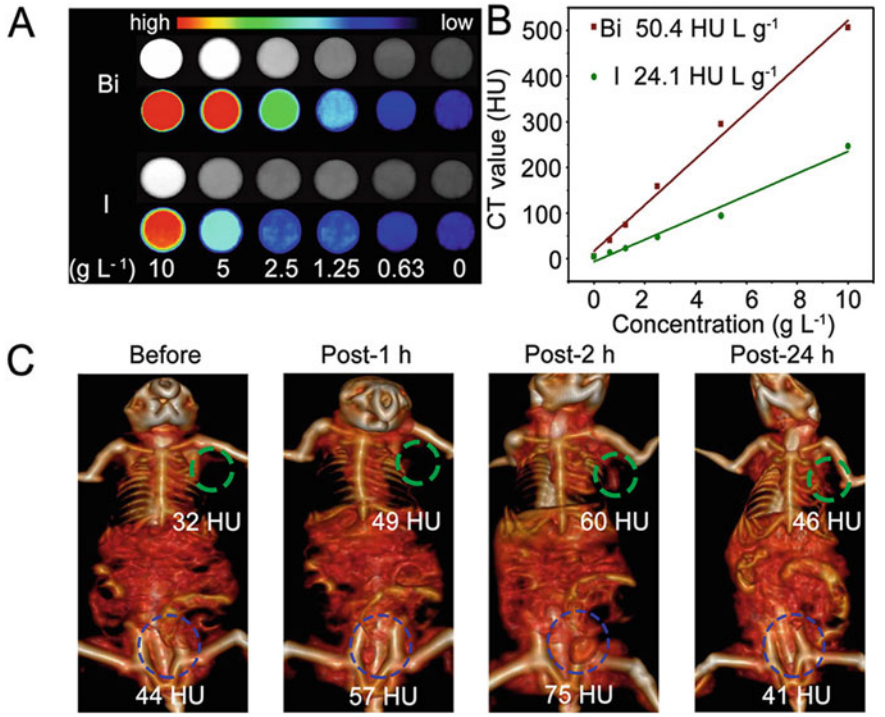

Fig. 10 **a** CT images of Bi and iohexol (I) for different concentrations from 0 to10 $g.L^{-1}$, **b** Quantification of CT value for Bi–Bi_2S_3/BSA&FA NPs and iohexol samples, **c** In vivo CT images of tumor (green circles) and bladder (blue circles). Reproduced with permission from Ref. [58]. Copyright 2019, with permission from ACS

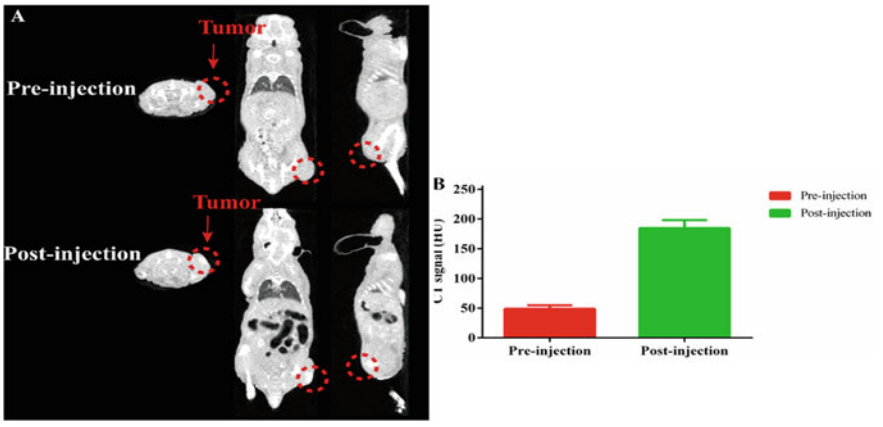

Fig. 11 In vivo CT imaging of BiF_3Ln@PVP NPs, **a** CT images before and after the injection of BiF_3Ln@PVP NPs (tumor site is shown in red circle), **b** Corresponding CT values (HU). Reproduced from Ref. [61] with the permission of the Creative Commons Attribution 4.0 International License (http://creativecommons.org/licenses/by/4.0/). Copyright 2021, Springer

Table 2 Risk of malignancy after thorotrast administration

Type of tumor	Related organ	Model of injection	Human or animal	References
Angiosarcoma[4]	Liver	Intravenous	Human	[69–71]
Plasmacytoma[5]	Blood	–	Human	[72–74]
Anaplastic[6]	Lung	–	Human	[74]
Sarcoma	–	Intraperitoneal	Guinea pigs	[75]
Cholangiocarcinoma[7]	Liver	Intravenous	Hamsters	[75]
Fibrosarcoma[8]	Local	Subcutaneous	Mice	[75]
Hemangioendotheliosarcoma[9]	Liver	Intravenous	Rabbits	[76]
Adenomas[10]	Liver	Intravenous	Rats	[77]

2.4 Thorium Oxide Nanoparticle Based Contrast Agents

Thorium, one of the actinide group element (group 4, period 7) with a high atomic number of 90 is represented with the symbol Th. In 1828, Jöns Jacob Berzelius, a Swedish scientist, discovered Th in the mineral thorite ($ThSiO_4$). Heyden chemical company produced colloidal thorium oxide (ThO_2) as a radiological contrast agent in 1920s [62, 63]. Favorably, ThO_2 or Thorotrast (trade label) does not aggregate after intravenous administration with a size of 3–10 nm and showed appropriate contrast agent performance due to the high atomic weight. ThO_2 was also used as oral administration in gastric mucosa and upper part of gut for imaging applications. However, it is found that ThO_2 not only deposits lifelong in the RES of many organs such as spleen, liver, lymph nodes and bone marrow, but also causes formation of malignant tumors, blood dyscrasias, liver fibrosis and leukemia [64–68]. Table 2 shows some of these problems which cause malignant effects in human and animal models [65]. Later, the usage of colloidal ThO_2 was eventually abandoned due to the severe toxicity.

[4] Angiosarcoma is a rare cancer that develops in the inner lining of blood vessels and lymph vessels. This cancer can occur anywhere in the body but most often is in the skin, breast, liver and spleen.

[5] Plasmacytoma is a plasma cell dyscrasia in which a plasma cell tumor grows within soft tissue or within the axial skeleton.

[6] A term used to describe cancer cells that divide rapidly and have little or no resemblance to normal cells.

[7] Cholangiocarcinoma is a type of cancer that forms in the slender tubes (bile ducts) that carry the digestive fluid bile. Bile ducts connect your liver to your gallbladder and to your small intestine.

[8] Fibrosarcoma is a rare type of cancer that affects cells known as fibroblasts. Fibroblasts are responsible for creating the fibrous tissue found throughout the body. Tendons, which connect muscles to bones, are made up of fibrous tissue.

[9] A malignant tumor arising from vascular tissue.

[10] Adenoma is a benign tumor of glandular tissue, such as the mucosa of stomach, small intestine, and colon, in which tumor cells form glands or gland like structures.

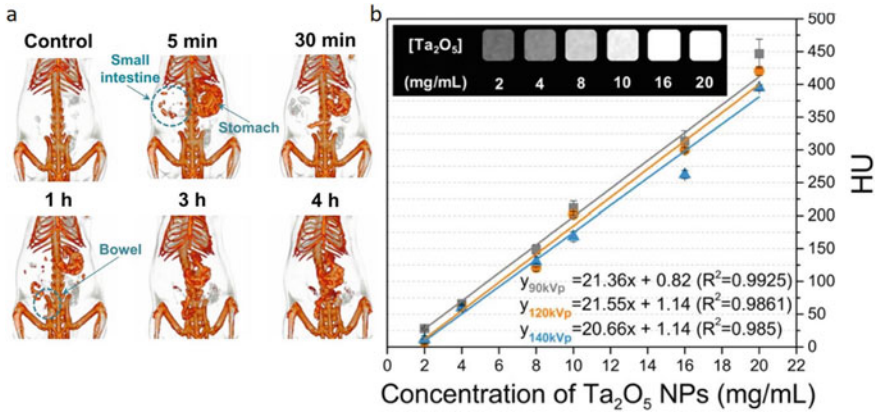

Fig. 12 **a** CT image of Ta_2O_5 NPs from the coronal views in GI tract, **b** CT images and values of Ta_2O_5. Reproduced with permission from Ref. [84]. Copyright 2020, with permission from RSC

2.5 Tantalum Nanoparticle Based Contrast Agents

Tantalum is a chemical element with the atomic number of 73 and the symbol Ta in the periodic table. Tantalum has demonstrated certain benefits over traditional iodinated contrast agents as a X-ray contrast agent due to the high radiopacity with a density of 16.6 g/mL [78–80]. Tantalum oxide (Ta_2O_5) is a biocompatible material and used in gastrointestinal imaging and angiography [81–83]. Bonitatibus et al. designed a tantalum-based NP in the form of a core–shell structure with the total size of less than 6 nm. Silica was used as a coating layer to make NPs stable and water soluble. In vivo experiment showed that tantalum-based NPs displayed appropriate contrast compared to iodine [84]. Krivoshapkin and his colleagues also showed Ta_2O_5 NPs, at a concentration of 20 $mg.ml^{-1}$, can increase CT value from 47.1 ± 5.7 HU to 426.1 ± 2.8 HU at tumor site in 10 min Fig. 12 [85].

2.6 Rare Earth Nanoparticles Based Contrast Agents

Rare earth elements display very complex luminescence activity which arises from f-f transitions of the 4f shell and f-d transitions in the 4f-5d shell. Upconversion nanoparticles (UCNPs) and downconversion nanoparticles (DCNPs) are the two primary types of rare-earth based NPs. UCNPs can convert low energy with long-wavelength light to high energy with short wavelength while DCNPs convert high energy to low energy. Rare-earth NPs have been widely employed in vitro and in vivo imaging of biomolecules due to the outstanding properties of rare-earth ions, such as their low energy losses, different absorption and emission wavelengths, and low

photobleaching [86]. Below, two rare-earth NPs are introduced as contrast agents in imaging applications.

2.6.1 Gadolinium Based Nanoparticles

Gadolinium (Gd) is an appropriate contrast agent for MRI [87] and CT imaging due to its high atomic number (64), large number of unpaired electrons and high K-edge (52 keV) which is greater than iodine. Havoron et al. evaluated Gd oxide as a contrast agent in 1970s. Their animal test resulted that there were no observable toxic effects when poly(vinylpyrrolidone) was used to stabilize the Gd_2O_3 microparticles [88, 89]. In a study, Prosser et al. used Gd NPs in both CT and MRI applications. Their data indicated that $NaGdF_4$ (with a low polydispersity and 20–22 nm size) and 50:50 mixture of GdF_3 and CeF_3 (with the 10–12 nm size) not only displayed high relaxivities at 1.5 and 3 T (35–40 $mL.s^{-1}$ mg^{-1}) in MRI which was better than Gd^{3+}-DTPA (gadopentetate dimeglumine, Magnevist®) complex but also could be functionalized with folic acid for targeting purpose in human cancer cells [90].

In another study, Watkin et al. described Gd_2O_3-albumin NPs with a diameter of 20–40 nm and embedded them within protein microspheres as CT contrast agent, which had 40 to 100 times higher contrast effect than iopamidol[11] at the same concentration [91, 92]. In a similar approach, Ru(bpy):Gd(III)@SiO_2 NPs were developed as a contrast agent for CT imaging, MRI and diffuse optical tomography. Ru(bpy) can act as a dye to prohibit photo bleaching and Gd has paramagnetic properties which is useful in enhancing MR contrast for both longitudinal (T_1) and transverse (T_2) proton relaxation rate measurements. NPs displayed higher contrast enhancement than the commercial contrast agent, Gadoteridol, however, the contrast effect was less than the trade mark Omnipaque® at the same concentration [27, 93].

Qui et al. explored fabrication of neodymium (Nd)-doped and gadolinium tungstate NPs with a hydrophilic layer ($NaGd(WO_4)_2$:Nd@PDA–HA NPs) for CT, MRI and fluorescence imaging. Their result demonstrated that NPs displayed a higher CT contrast (11.67 ± 0.46 $HU.mM^{-1}$) compared to the commercial contrast agent, iohexol (4.31 ± 0.09 $HU.mM^{-1}$). NPs were proposed as an appropriate CT contrast agent in breast tumor at a concentration of 2.5 $mg.mL^{-1}$ [94].

2.6.2 Holmium Based Nanoparticles

Holmium with electron configuration of [Xe] 4f11 6s2 is soft and stable in the room temperate but it oxidizes rapidly in moisture. Similar to gadolinium, it exhibits an effective contrasting agent for both MRI and CT imaging due to its paramagnetic nature, high atomic number (67) and high attenuation coefficient [95–98]. Bult et al. synthesized HoAcAc NPs (Fig. 13a) by dissolving holmium acetylacetonate

[11] Iopamidol, sold under the brand name Isovue among others, is a nonionic, low-osmolar iodinated contrast agent, developed by Bracco Diagnostics.

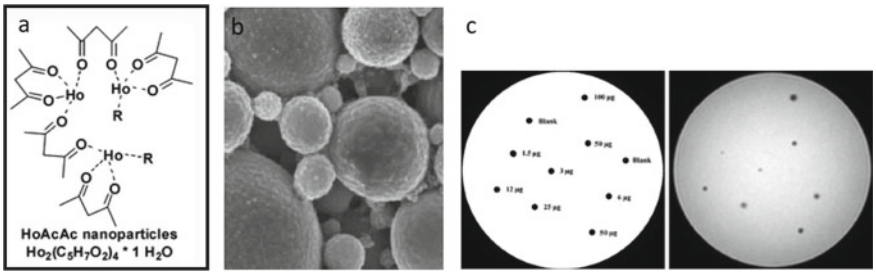

Fig. 13 **a** Structure of HoAcAc NPs, **b** STEM image of HoAcAc NPs with the size of 78 ± 10 nm, **c** Phantom image (left) and photograph of HoAcAc NPs at different concentration. Reproduced from Ref. [99] with the permission of the Creative Commons Attribution Noncommercial License (https://creativecommons.org/licenses/by-nc/2.0). Copyright 2010, Springer

in chloroform, followed by emulsifying in an aqueous surfactant solution, and stabilizing with polyvinyl alcohol and didodecyldimethylammonium bromide. Spherical HoAcAc NPs had a diameter of 78 ± 10 nm (Fig. 13b) and had higher CT contrast effect (15.6 HU·mg^{-1}) in comparison to the iodine. Figure 13c shows agarose MRI phantom images for different NP concentration, where increase in the amount of NPs resulted in an increase in the degree of darkness [99].

Ocana et al. explored the role of dysprosium vanadate ($DyVO_4$) and holmium vanadate ($HoVO_4$) NPs functionalized with poly(acrylic acid) (PAA) with a diameter of 60 nm for contrast agent application. Such NPs displayed (Fig. 14) 2.4 fold more contrast than the commercial agent iohexol [98].

Cormode et al. used cerium oxide NPs as a CT contrast agent with k-edge of 40.4 keV for imaging the gastrointestinal tract (GIT) and inflammatory bowel disease (IBD). Dextran was used to increase the accumulation in the IBD inflammation sites.

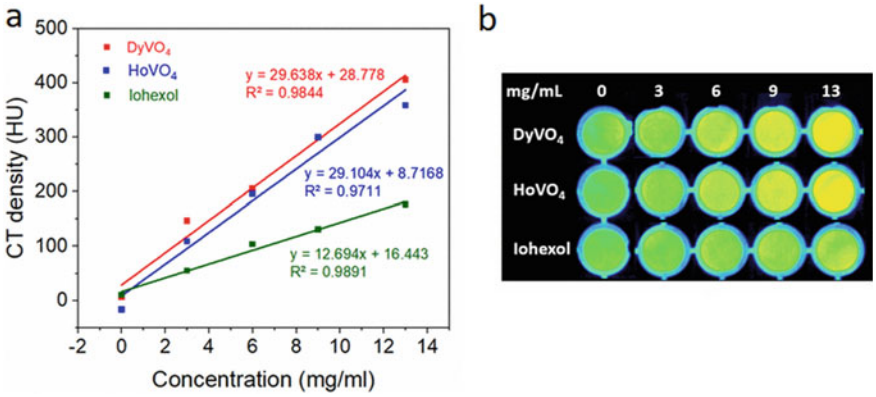

Fig. 14 **a** Quantification of HU for HVO_4 and $DyVO_4$ NPs functionalized with PAA in comparison to the iohexol, **b** CT phantom images for different NP concentrations. Reproduced with permission from Ref. [98]. Copyright 2020, with permission from ACS

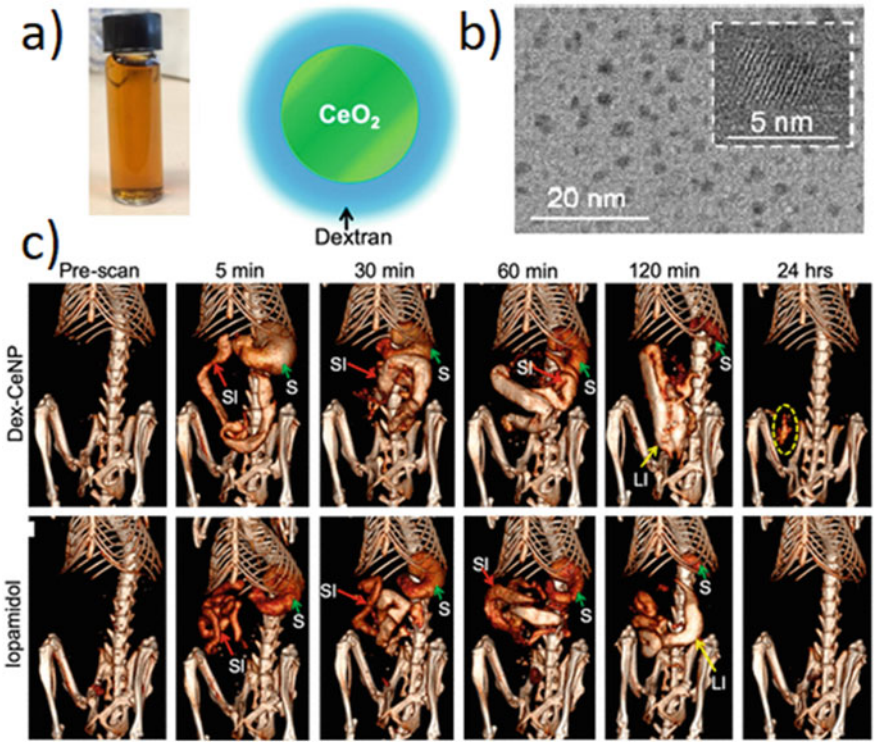

Fig. 15 **a** Photograph of a solution of Dex-CeNP, and schematic illustration of Dex-CeNF, **b** TEM image of Dex-CeNP, and **c** Micro-CT images of colitis mice, before and after oral administration of Dex-CeNP and iopamidol where "S", "SI" and "LI" are the stomach, small intestine, and large intestine, respectively. The yellow arrow shows Dex-CeNP accumulation in a colitis site. Reproduced with permission from Ref. [100]. Copyright 2020, with permission from ACS

Dextran-coated cerium oxide NPs (Dex-CeNP) was compared to the FDA-approved commercial contrast agent iopamidel (Fig. 15). More than 97% of oral dosage of Dex-CeNP was eliminated from the body within 24 h. Therefore, Dex-CeNP has the potential to be used as a CT contrast agent for GIT imaging in IBD [100].

3 Conclusion and Future Perspective

Advances in CT equipment, along with better CT contrast formulations are propelling the field of CT imaging forward in both laboratory and clinic throughout the world. Contrast enhancement and high-resolution CT images, as well as the low cost and widespread availability of clinical CT scanners facilitate the diagnosis process. High atomic number based NP based contrast agents can be a prosperous milestone in the CT imaging to decrease the radiation doses while maintaining sensitivity and

specificity, simultaneously. The reviewed studies displayed novel metal NPs can be appropriate candidates as contrast agents in CT imaging and MRI applications in compared to the traditional iodine-based contrast agent as long as long-term side effects are evaluated precisely in the clinical phase to prevent possible health concerns. Furthermore, the ability to integrate imaging and treatment as a theranostic approach in a single nanoplatform is another promising approach in biomedical applications. Appropriate design and functionalization of nanostructures can target specific tissue/cell for imaging and therapy aims. Future research and development of novel CT contrast agents is expected to result in new chemical structures, modes of different functionality, and improved image resolution, and nanoparticle based commercial CT contrast agents could be possible as long as long term in vivo concerns are well documented.

References

1. Lu L, et al (2021) High energy X-ray radiation sensitive scintillating materials for medical imaging, cancer diagnosis and therapy. Nano Energy 79:105437
2. Chen H, Rogalski MM, Anker JN (2012) Advances in functional X-ray imaging techniques and contrast agents. Phys Chem Chem Phys 14(39):13469–13486
3. Terao Y, et al (2021) X-ray induced luminescence spectroscopy for DNA damaging intermediates aided by a monochromatic synchrotron radiation. Int J Radiat Biol 1–6
4. Wang X et al (2021) Organic phosphors with bright triplet excitons for efficient X-ray-excited luminescence. Nat Photonics 15(3):187–192
5. Sy S et al (2010) Terahertz spectroscopy of liver cirrhosis: investigating the origin of contrast. Phys Med Biol 55(24):7587
6. Ji Z et al (2012) Three-dimensional thermoacoustic imaging for early breast cancer detection. Med Phys 39(11):6738–6744
7. Ma J, et al (2012) Variance analysis of x-ray CT sinograms in the presence of electronic noise background. Med Phys 39(7Part1):4051–4065
8. Cheong S-K et al (2010) X-ray fluorescence computed tomography (XFCT) imaging of gold nanoparticle-loaded objects using 110 kVp x-rays. Phys Med Biol 55(3):647
9. Bonekamp D, Hammoud DA, Pomper MG (2010) Molecular imaging: techniques and current clinical applications. Appl Radiol 39(5):10
10. Nosrati H et al (2022) Complete ablation of tumors using synchronous chemoradiation with bimetallic theranostic nanoparticles. Bioactive Mater 7:74–84
11. Birnbacher L et al (2018) Accurate effective atomic number determination with polychromatic grating-based phase-contrast computed tomography. Opt Express 26(12):15153–15166
12. Spiers F (1946) Effective atomic number and energy absorption in tissues. Br J Radiol 19(218):52–63
13. Lu W, Mackie TR (2002) Tomographic motion detection and correction directly in sinogram space. Phys Med Biol 47(8):1267
14. Meija J et al (2016) Atomic weights of the elements 2013 (IUPAC Technical Report). Pure Appl Chem 88(3):265–291
15. Hainfeld JF, Slatkin DN, Smilowitz HM (2004) The use of gold nanoparticles to enhance radiotherapy in mice. Phys Med Biol 49(18):N309
16. Popovtzer R et al (2008) Targeted gold nanoparticles enable molecular CT imaging of cancer. Nano Lett 8(12):4593–4596
17. Turkevich J, Stevenson PC, Hillier J (1951) A study of the nucleation and growth processes in the synthesis of colloidal gold. Discuss Faraday Soc 11:55–75

18. Watson KJ et al (1999) Hybrid nanoparticles with block copolymer shell structures. J Am Chem Soc 121(2):462–463
19. Kim D et al (2007) Antibiofouling polymer-coated gold nanoparticles as a contrast agent for in vivo X-ray computed tomography imaging. J Am Chem Soc 129(24):7661–7665
20. Cai Q-Y et al (2007) Colloidal gold nanoparticles as a blood-pool contrast agent for X-ray computed tomography in mice. Invest Radiol 42(12):797–806
21. Xiao M et al (2009) Gold nanotags for combined multi-colored Raman spectroscopy and x-ray computed tomography. Nanotechnology 21(3):035101
22. Eck W et al (2010) Anti-CD4-targeted gold nanoparticles induce specific contrast enhancement of peripheral lymph nodes in X-ray computed tomography of live mice. Nano Lett 10(7):2318–2322
23. Yonezawa T, Kunitake T (1999) Practical preparation of anionic mercapto ligand-stabilized gold nanoparticles and their immobilization. Colloids Surf, A 149(1–3):193–199
24. Hainfeld J et al (2006) Gold nanoparticles: a new X-ray contrast agent. Br J Radiol 79(939):248–253
25. Sokolov K et al (2003) Optical systems for in vivo molecular imaging of cancer. Technol Cancer Res Treat 2(6):491–504
26. Hainfeld JF et al (2011) Micro-CT enables microlocalisation and quantification of Her2-targeted gold nanoparticles within tumour regions. Br J Radiol 84(1002):526–533
27. Jakhmola A, Anton N, Vandamme TF (2012) Inorganic nanoparticles based contrast agents for X-ray computed tomography. Adv Healthcare Mater 1(4):413–431
28. Sun IC, et al (2009) Heparin-coated gold nanoparticles for liver-specific CT imaging. Chem A Europ J 15(48):13341–13347
29. Boote E et al (2010) Gold nanoparticle contrast in a phantom and juvenile swine: models for molecular imaging of human organs using x-ray computed tomography. Acad Radiol 17(4):410–417
30. Shi X et al (2007) Dendrimer-entrapped gold nanoparticles as a platform for cancer-cell targeting and imaging. Small 3(7):1245–1252
31. Alric C et al (2008) Gadolinium chelate coated gold nanoparticles as contrast agents for both X-ray computed tomography and magnetic resonance imaging. J Am Chem Soc 130(18):5908–5915
32. Park J-A et al (2010) Gold nanoparticles functionalized by gadolinium–DTPA conjugate of cysteine as a multimodal bioimaging agent. Bioorg Med Chem Lett 20(7):2287–2291
33. Kim H-K et al (2010) Gold nanoparticles coated with gadolinium-DTPA-bisamide conjugate of penicillamine (Au@ GdL) as a T1-weighted blood pool contrast agent. J Mater Chem 20(26):5411–5417
34. Shaikh MN (2013) Thiolated Gd (III) chelate coated gold nanoparticles: synthesis, characterization, x-ray CT and MRI relaxivity studies. In: Materials Science Forum. 2013. Trans Tech Publ
35. Kim D et al (2011) Amphiphilic polymer-coated hybrid nanoparticles as CT/MRI dual contrast agents. Nanotechnology 22(15):155101
36. Kim D-K et al (2009) Antibiofouling polymer coated gold@ iron oxide nanoparticle (GION) as a dual contrast agent for CT and MRI. Bull Korean Chem Soc 30(8):1855–1857
37. van Schooneveld MM, Hart DC't, Fayad ZA, Mulder WJM, Meijerink A (2010) Contrast Media Mol. Imaging 5:231–236
38. Mohajeri M et al (2020) Pegylated deoxycholic acid coated gold nanoparticles as a highly stable CT contrast agent. ChemistrySelect 5(29):9119–9126
39. Gao Y et al (2020) Use of the highly biocompatible Au nanocages@ PEG nanoparticles as a new contrast agent for in vivo computed tomography scan imaging. Nanoscale Res Lett 15(1):1–9
40. Park Y-S et al (2007) Concentrated colloids of silica-encapsulated gold nanoparticles: colloidal stability, cytotoxicity, and X-ray absorption. J Nanosci Nanotechnol 7(8):2690–2695
41. Huang P et al (2011) Folic acid-conjugated silica-modified gold nanorods for X-ray/CT imaging-guided dual-mode radiation and photo-thermal therapy. Biomaterials 32(36):9796–9809

42. Aslan N, et al (2020) Metallic nanoparticles as X-Ray computed tomography (CT) contrast agents: a review. J Mol Struct 1219:128599
43. Liu R et al (2021) Multifunctional core-shell tecto dendrimers incorporated with gold nanoparticles for targeted dual mode CT/MR imaging of tumors. ACS Appl Bio Mater 4(2):1803–1812
44. Karunamuni R, et al (2012) An examination of silver as a radiographic contrast agent in dual-energy breast X-ray imaging. In: International Workshop on Digital Mammography. Springer
45. Voelcker F, Von Lichtenberg A (1906) Pyelographie (Röntgenographie des Nierenbeckens nach Kollargolfüllung). Munch Med Wochenschr 53:105–106
46. Swick M (1978) Radiographic media in urology: the discovery of excretion urography: historical and developmental aspects of the organically bound urographic media and their role in the varied diagnostic angiographic areas. Surg Clin North Am 58(5):977–994
47. Skrepetis K, Siafakas I, Lykourinas M (2001) Evolution of retrograde pyelography and excretory urography in the early 20th century. J Endourol 15(7):691–696
48. Seltzer SE, Adams DF, Davis MA, Hessel SJ, Paskins-Hurlburt AJ, Havron A, Hollenberg NK (1979) Invest Radiol 14:356
49. Nieves LM et al (2021) Silver telluride nanoparticles as biocompatible and enhanced contrast agents for X-ray imaging: an in vivo breast cancer screening study. Nanoscale 13(1):163–174
50. Zhou Z et al (2021) Construction of smart nanotheranostic platform Bi-Ag@ PVP: multimodal CT/PA imaging-guided PDT/PTT for cancer therapy. ACS Omega 6(16):10723–10734
51. Yu S-B, Watson AD (1999) Metal-based X-ray contrast media. Chem Rev 99(9):2353–2378
52. Rumpel T (1897) The clinical diagnosis of fusiform dilatation of the esophagus. Muenchen Med Wschr 44:420–421
53. Rabin O et al (2006) An X-ray computed tomography imaging agent based on long-circulating bismuth sulphide nanoparticles. Nat Mater 5(2):118–122
54. Barnett B et al (2006) Radiopaque alginate microcapsules for X-ray visualization and immunoprotection of cellular therapeutics. Mol Pharm 3(5):531–538
55. Liu Q et al (2021) Pharmacological ascorbate promotes the tumor radiosensitization of Au@ Pd nanoparticles with simultaneous protection of normal tissues. ACS Appl Bio Mater 4(2):1843–1851
56. Fu W et al (2020) Stimuli-responsive small-on-large nanoradiosensitizer for enhanced tumor penetration and radiotherapy sensitization. ACS Nano 14(8):10001–10017
57. Pan D et al (2010) Computed tomography in color: NanoK-enhanced spectral CT molecular imaging. Angew Chem 122(50):9829–9833
58. Dong L et al (2019) Renal clearable Bi–Bi2S3 heterostructure nanoparticles for targeting cancer theranostics. ACS Appl Mater Interfaces 11(8):7774–7781
59. Zhang F et al (2020) X-ray-triggered NO-released Bi–SNO nanoparticles: all-in-one nano-radiosensitizer with photothermal/gas therapy for enhanced radiotherapy. Nanoscale 12(37):19293–19307
60. Liu J et al (2021) Bi/Se-based nanotherapeutics sensitize CT image-guided stereotactic body radiotherapy through reprogramming the microenvironment of hepatocellular carcinoma. ACS Appl Mater Interfaces 13(36):42473–42485
61. Xie J et al (2021) Facile fabrication of BiF3: Ln (Ln= Gd, Yb, Er)@ PVP nanoparticles for high-efficiency computed tomography imaging. Nanoscale Res Lett 16(1):1–10
62. Abbatt JD (1979) History of the use and toxicity of thorotrast. Environ Res 18(1):6–12
63. Wickleder MS, Fourest B, Dorhout PK (2008) Thorium. The chemistry of the actinide and transactinide elements. Springer, pp 52–160
64. Ritter J, Rattner I (1932) Umbrathor in urography. Am J Roentgenol Rad Ther 28:629–633
65. Lipshutz GS, Brennan TV, Warren RS (2002) Thorotrast-induced liver neoplasia: a collective review. J Am Coll Surg 195(5):713–718
66. Cannon WB (1898) The movements of the stomach studied by means of the Rontgen rays. Am J Physiol Legacy Content 1(3):359–382

67. Lambrianides A, Askew A, Lefevre I (1986) Thorotrast-associated mucoepidermoid carcinoma of the liver. Br J Radiol 59(704):791–792
68. Md YI et al (1988) Pathomorphologic characteristics of 102 cases of thorotrast-related hepatocellular carcinoma, cholangiocarcinoma, and hepatic angiosarcoma. Cancer 62(6):1153–1162
69. MacMahon HE, Murphy AS, Bates MI (1947) Endothelial-cell sarcoma of liver following thorotrast injections. Am J Pathol 23(4):585
70. Andersson M et al (1994) Primary liver tumors among Danish patients exposed to Thorotrast. Radiat Res 137(2):262–273
71. Lee FI et al (1996) Malignant hepatic tumours associated with previous exposure to Thorotrast: four cases. Eur J Gastroenterol Hepatol 8(11):1121–1124
72. Kamiyama R et al (1988) Clinicopathological study of hematological disorders after Thorotrast administration in Japan. Blut 56(4):153–160
73. Mole R (1986) Leukaemia induction in man by radionuclides and some relevant experimental and human observations. Radiobiol Radium Thorotrast
74. Silva IDS, et al (1999) Mortality in the Portuguese thorotrast study. Radiat Res 152(6s): S88–S92
75. Wegener K (1979) Systematic review of thorotrast data and facts: animal experiments. Virchows Archiv A 381(3):245–268
76. Johansen C (1967) Tumors in rabbits after injection of various amounts of thorium dioxide. Ann NY Acad Sci 145:724–727
77. Wegener K, Hasenöhrl K, Wesch H (1983) Recent results of the German Thorotrast study–pathoanatomical changes in animal experiments and comparison to human thorotrastosis. Health Phys 44:307–316
78. Dilley RB, Nadel JA (1970) Powdered tantalum: its use as a roentgenographic contrast material. Ann Otol Rhinol Laryngol 79(5):945–952
79. Gamsu G, Nadel JA (1972) New technique for roentgenographic study of airways and lungs using powdered tantalum. Cancer 30(5):1353–1357
80. Gamsu G et al (1973) Powdered tantalum as a contrast agent for tracheobronchography in the pediatric patient. Radiology 107(1):151–157
81. Hallouard F, Lahiani-Skiba M, Skiba M (2015) Nanometric carriers or metallic nanoparticles: promising platforms for computed tomography applications. American Scientific Publishers
82. Goldberg HI, Dodds WJ, Jenis EH (1970) Experimental esophagitis: roentgenographic findings after insufflation of tantalum powder. Am J Roentgenol 110(2):288–294
83. Chakravarty S et al (2020) Tantalum oxide nanoparticles as versatile contrast agents for X-ray computed tomography. Nanoscale 12(14):7720–7734
84. Bonitatibus PJ Jr et al (2010) Synthesis, characterization, and computed tomography imaging of a tantalum oxide nanoparticle imaging agent. Chem Commun 46(47):8956–8958
85. Koshevaya E et al (2020) Surfactant-free tantalum oxide nanoparticles: synthesis, colloidal properties, and application as a contrast agent for computed tomography. J Mater Chem B 8(36):8337–8345
86. Yu Z, Eich C, Cruz LJ (2020) Recent advances in rare-earth-doped nanoparticles for NIR-II imaging and cancer theranostics. Front Chem 8:496
87. Ertas YN et al (2015) Oxide-free gadolinium nanocrystals with large magnetic moments. Chem Mater 27(15):5371–5376
88. Havron A et al (1980) Heavy metal particulate contrast materials for computed tomography of the liver. J Comput Assist Tomogr 4(5):642–648
89. Lu R et al (2020) Gadolinium-hyaluronic acid nanoparticles as an efficient and safe magnetic resonance imaging contrast agent for articular cartilage injury detection. Bioactive Mater 5(4):758–767
90. Cheung ENM et al (2010) Polymer-stabilized lanthanide fluoride nanoparticle aggregates as contrast agents for magnetic resonance imaging and computed tomography. Chem Mater 22(16):4728–4739
91. McDonald MA, Watkin KL (2003) Small particulate gadolinium oxide and gadolinium oxide albumin microspheres as multimodal contrast and therapeutic agents. Invest Radiol 38(6):305–310

92. Watkin KL, McDonald MA (2002) Multi-modal contrast agents: a first step. Acad Radiol 9(2):S285–S289
93. Santra S, walter GA, tan W, Moudgil BM, Mericle RA, et al (2005) Synthesis and characeterization of fluorescent, radio-opaque, and paramagnetic silica nanoparticles for multimodal bioimaging applications. Adv Mater 17:2165–2169
94. Yu X et al (2021) Integrating the second near-infrared fluorescence imaging with clinical techniques for multimodal cancer imaging by neodymium-doped gadolinium tungstate nanoparticles. Nano Res 14(7):2160–2170
95. Chang X et al (2020) Graphene oxide/BaHoF5/PEG nanocomposite for dual-modal imaging and heat shock protein inhibitor-sensitized tumor photothermal therapy. Carbon 158:372–385
96. Marasini S, et al (2021) Synthesis, characterizations, and 9.4 Tesla T2 MR images of polyacrylic acid-coated terbium (III) and holmium (III) oxide nanoparticles. Nanomaterials 11(5):1355
97. Zhai T et al (2020) Hollow bimetallic complex nanoparticles for trimodality imaging and photodynamic therapy in vivo. ACS Appl Mater Interfaces 12(33):37470–37476
98. Gómez-Gónzalez E et al (2020) Dysprosium and holmium vanadate nanoprobes as high-performance contrast agents for high-field magnetic resonance and computed tomography imaging. Inorg Chem 60(1):152–160
99. Bult W et al (2010) Holmium nanoparticles: preparation and in vitro characterization of a new device for radioablation of solid malignancies. Pharm Res 27(10):2205–2212
100. Naha PC et al (2020) Dextran-coated cerium oxide nanoparticles: a computed tomography contrast agent for imaging the gastrointestinal tract and inflammatory bowel disease. ACS Nano 14(8):10187–10197